SPACE SCIENCES

The structure of a complex, asymmetric coronal mass ejection revealed by 17 spacecraft across the inner heliosphere

Adrienn Luspay-Kuti[1]*, Drew L. Turner[1], Evangelos Paouris[1], Angelos Vourlidas[1], Alexander B. Crew[1], Ralph L. McNutt[1], Joseph H. Westlake[2], Savvas Raptis[1], Corey J. Cochrane[3], Xianzhe Jia[4], Carol A. Raymond[3], Haje Korth[1], Daniel Heyner[5], Kathleen Hanley[6], Ali Rahmati[6], Jacob R. Gruesbeck[7], Jasper S. Halekas[8], Shannon M. Curry[9], Howard Todd Smith[1], Michael L. Stevens[10], Elias Roussos[11], Kathleen E. Mandt[7], Margaret G. Kivelson[12,13]†, James A. Slavin[4]†, Dany Waller[1,14]†, Krishan K. Khurana[12]†, Tom Andre Nordheim[1]†, Carol S. Paty[15]†, Abigail M. Rymer[1]†, Joachim Saur[16]†, Norbert Krupp[11]†

Coronal mass ejections (CMEs) are enormous bursts of plasma and magnetic field from the Sun that propagate explosively through the Solar System. CMEs are the primary drivers of the most severe space-weather events, posing major radiation hazards for human exploration beyond Earth's magnetosphere, including missions to the Moon and Mars. During Europa Clipper's cruise between Earth and Mars, its Plasma Instrument for Magnetic Sounding (PIMS) recorded unusual solar-wind conditions later identified as the wake of a complex CME. Data from an unprecedented network of 17 spacecraft across the inner Solar System revealed a hidden Earth-directed component that propagated asymmetrically and could not have been predicted without off-Sun-Earth-line observations. This component also affected Europa Clipper and Mars, demonstrating how a missed forecast of this kind could endanger a crewed mission. These findings highlight the need for multipoint observations, including planetary missions in cruise, to improve space-weather forecasting, mission planning, and operations.

INTRODUCTION

NASA's flagship planetary mission, Europa Clipper, launched on 14 October 2024 and is now en route to Jupiter's ocean-world Europa via gravity assists at Mars (completed on 1 March 2025) and Earth (scheduled for 3 December 2026). Two of its 10 instruments, the Plasma Instrument for Magnetic Sounding (PIMS) and the Europa Clipper Magnetometer (ECM), will determine Europa's subsurface ocean thickness, conductivity (a proxy for salinity), and ice shell thickness (*1*).

On 19 December 2024, Europa Clipper was 1.19 astronomical units (au) from the Sun, outbound toward Mars and nearly aligned with Earth within the ecliptic plane. During a 1-hour instrument checkout, PIMS (*2*) collected solar wind data to confirm postlaunch performance. Meanwhile, ECM (*3*) continuously measured magnetic fields to monitor potential interference from spacecraft subsystems between 22 November 2024 and 22 January 2025 (*4*). Figure 1 shows selected Europa Clipper magnetic field and plasma measurements during this interval, including ECM data (Fig. 1, A to C) and the PIMS energy-time spectrogram obtained during the checkout period (Fig. 1D).

Examination of the PIMS data revealed that the sunward-facing PIMS cup detected ions between ~1450 and ~1700 eV (Fig. 1D), corresponding to fast solar wind (~530 to 570 km s^{-1} assuming protons). Because PIMS directly samples the energy of the incoming plasma, the spectrogram provides an immediate visual indication of changes in the solar wind speed, temperature, and density. The spectrogram in Fig. 1D displays a broad current peak and low intensity, indicative of low-density, high-temperature plasma relative to nominal solar wind conditions (*5*, *6*). These anomalous PIMS measurements prompted further investigation into the broader heliospheric context.

While these plasma characteristics are atypical for nominal solar wind at this heliocentric distance, they are commonly associated with coronal mass ejection (CME)–driven structures. At the time of the PIMS measurements, it was unclear whether the anomalous plasma reflected a CME wake, a flank encounter, or other transient solar wind variability. From the perspective of a single spacecraft, such plasma signatures do not uniquely identify the global structure behind them. Distinguishing among these possibilities requires multipoint observations.

Fortuitously, in December 2024, the inner heliosphere was covered by an unusually large and well-distributed fleet of 17 spacecraft, providing dense radial and longitudinal coverage. This configuration enabled reconstruction of the CME and revealed that the PIMS measurements captured only one portion of a structure far more complex than could be inferred from single-point observations. We begin at the Sun.

[1]Johns Hopkins University Applied Physics Laboratory, 11000 Johns Hopkins Rd., Laurel, MD 20723, USA. [2]NASA Headquarters Heliophysics SMD, 300 E Street SW, Suite 5R30, Washington, DC 20546, USA. [3]Jet Propulsion Laboratory, California Institute of Technology, 4800 Oak Grove Dr., Pasadena, CA 91109, USA. [4]University of Michigan, 500 S. State St., Ann Arbor, MI 48109, USA. [5]Braunschweig University of Technology, Universitätsplatz 2, 38106 Braunschweig, Germany. [6]University of California, Berkeley, 366 Physics North MC 7300, Berkeley, CA 94720, USA. [7]NASA Goddard Space Flight Center, 8800 Greenbelt Rd., Greenbelt, MD 20771, USA. [8]Department of Physics and Astronomy, University of Iowa, 30 N Dubuque St., Iowa City, IA 52242, USA. [9]Laboratory for Atmospheric and Space Physics, University of Colorado, Boulder, Boulder, CO 80303 USA. [10]Harvard Smithsonian Astrophysical Observatory, 60 Garden St., Cambridge, MA 02138, USA. [11]Max Planck Institute for Solar System Research, Justus-von-Liebig-Weg 3, 37077 Göttingen, Germany. [12]University of California, Los Angeles, 405 Hilgard Ave., Los Angeles, CA 90095, USA. [13]Department of Geophysics and Department of Earth and Planetary Sciences, Stanford Doerr School of Sustainability, Stanford University, Stanford, CA 94305, USA. [14]Department of Physics, Umeå University, Linnaeus väg 24, 907 36 Umeå, Sweden. [15]University of Oregon, 1585 E 13th Ave., Eugene, OR 97403, USA. [16]University of Cologne, Albertus-Magnus-Platz, 50923 Köln, Germany.
*Corresponding author. Email: adrienn.luspay-kuti@jhuapl.edu
†These authors contributed equally to this work.

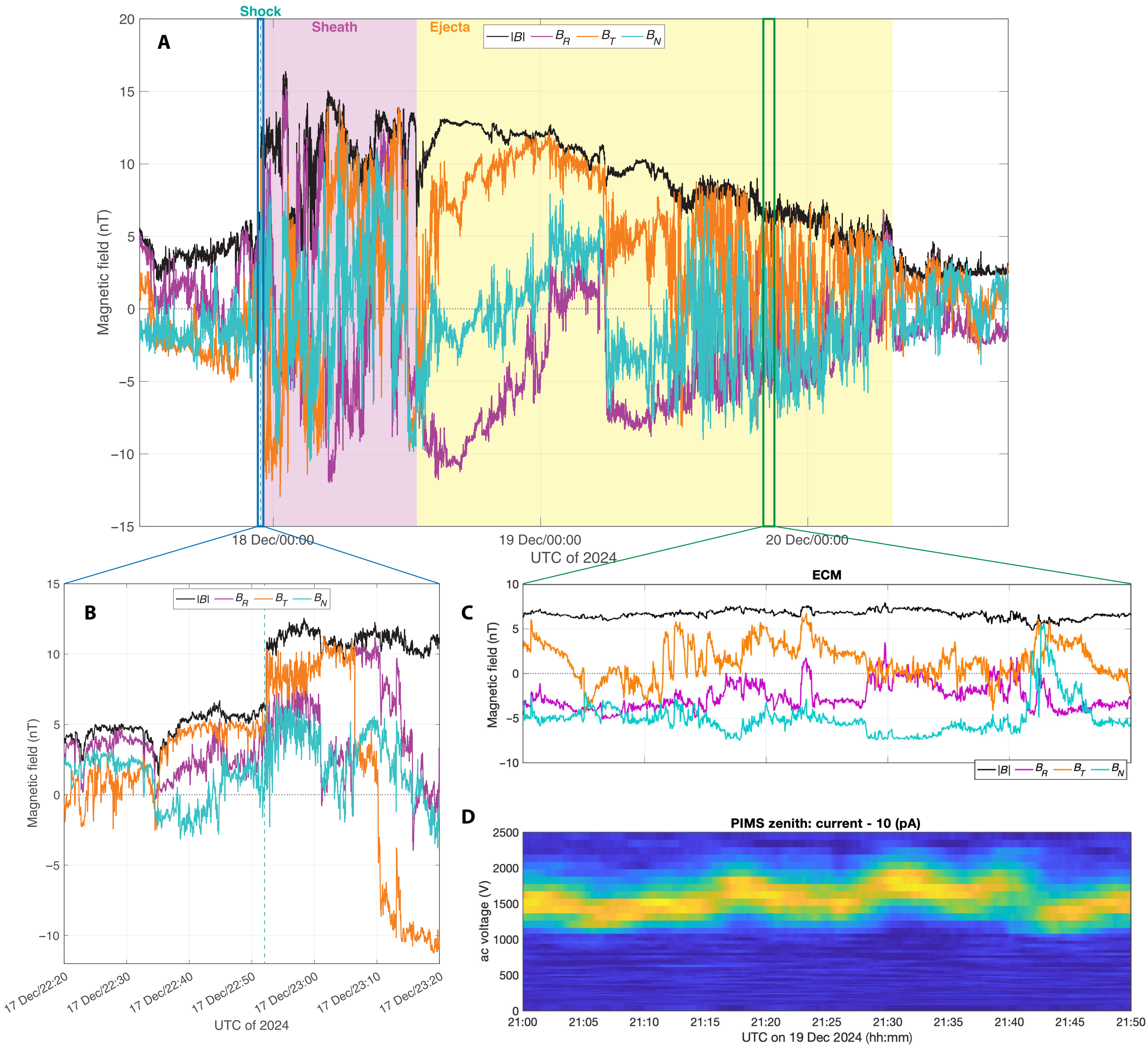

Fig. 1. PIMS plasma and ECM magnetic field measurements show anomalous solar wind conditions at Europa Clipper. (**A**) Calibrated magnetic field measurements from ECM, rotated into the spacecraft frame, over ~3-day interval. Shaded regions indicate the CME shock (blue box), sheath (lilac), and ejecta (yellow). The green box marks the PIMS interval shown in (D). (**B**) Magnetic field data showing a well-defined interplanetary shock at 22:52 UT on 17 December 2024. (**C**) Zoomed-in view of the magnetic field during the PIMS interval. (**D**) Energy-time spectrogram from the sunward-facing PIMS Faraday cup on 19 December 2024, 21:00 to 21:50 UT. Enhanced ion currents near 1500 eV (orange/yellow) correspond to fast solar wind (~530 to 570 km s^{-1}). The broadened, low-amplitude peak indicates lower densities and higher temperatures than nominal solar wind conditions. To improve signal statistics in this low signal-to-noise regime, a 64-point running average was applied, and a 10-pA background was subtracted. The currents are partially calibrated and do not represent absolute plasma flux or density. Together, these measurements show that Europa Clipper encountered CME ejecta under disturbed solar wind conditions, motivating reconstruction of the event using multipoint observations.

RESULTS

Solar origin and the hidden Earth-directed component

A slow CME was observed on 15 December at 00:48 UT in SOHO/LASCO C2 (*7*) and at ~01:53 UT in STEREO/SECCHI COR2 (*8*). The CME was associated with an extended quiet-Sun filament on the Earth-facing solar disk near 28° south latitude (Fig. 2, A and C), spanning more than 60° in longitude. The filament eruption persisted for over 4 hours, from 14 December at 22:30 UT to 15 December at 02:30 UT, and was accompanied by low-level flaring activity (GOES class C2-C5) in nearby active regions AR3924 (C2.6 at S16W15 and C4.2 at S17W22) and AR3917 (C2.6 at S14W78). These flares occurred concurrently with the filament eruption and were likely associated with the CME's onset.

The CME propagated southward from the ecliptic plane (Fig. 2B, green wireframe), but it was sufficiently wide to produce a flank encounter with STEREO-A and possibly Earth. STEREO-A/COR2

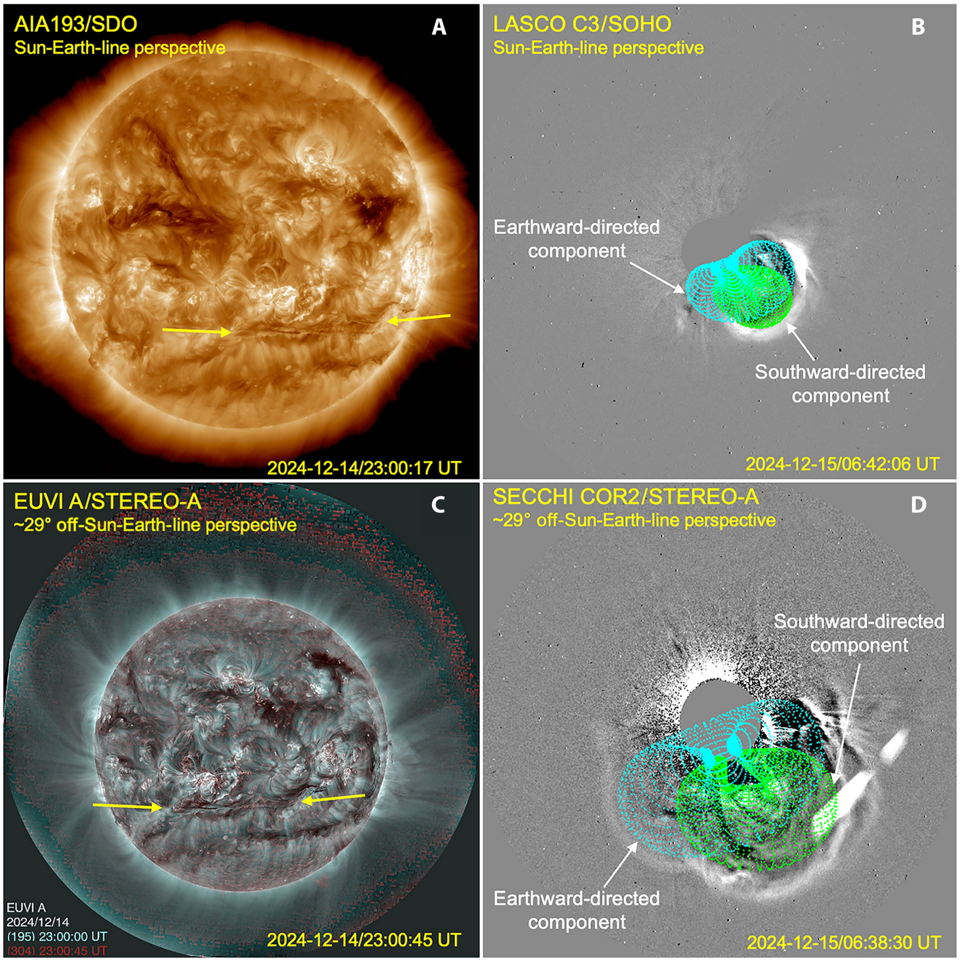

Fig. 2. Extreme ultraviolet (EUV) and coronagraph observations of the solar disk and corona highlighting the extended filament that produced the complex CME. (**A**) SDO/AIA 193-Å image from the Sun-Earth line on 14 December 2024 at 23:00 UT. (**C**) STEREO-A/EUVI view of the same region from ~29° off the Sun-Earth line on 15 December 2024 at 23:00 UT. (**B**) SOHO/LASCO C3 coronagraph image from the Sun-Earth line on 15 December 2024 at 06:42 UT. (**D**) STEREO-A/COR2 coronagraph image from ~29° off the Sun-Earth line on 15 December 2024 at 06:38 UT. The occulting disk radii are ~3.7 solar radii (LASCO C3) and ~2.7 solar radii (COR2). Colored overlays show the three-dimensional reconstruction of CME structure. When viewed along the Sun-Earth line, the Earth-directed component (cyan) is fully superposed on a southward-directed component (green), completely obscuring it in the SOHO/LASCO view. From the STEREO-A, vantage point, however, the two components separate clearly, revealing the previously hidden Earth-directed expansion. The reconstruction demonstrates that the event was a single CME with intrinsically distinct directional components, including an Earth-directed component invisible from the Sun-Earth line.

images (Fig. 2D, cyan wireframe) show the east flank of the event; from the Sun-Earth line, this Earth-directed flank was obscured by the dominant southward-propagating portion of the CME (Fig. 2B). Consequently, the Earth-directed component was indistinguishable from the dominant southward-directed CME when viewed from the Sun-Earth perspective (hereafter referred to as the "hidden" or Earth-directed component).

STEREO-A COR2 captured the Earth-directed front at 01:55 UT on 15 December 2024. Positioned ~29° west of the Sun-Earth line (Fig. 2D), STEREO-A provided the crucial side-on perspective that revealed this otherwise hidden component. Without that vantage point, the Earth-directed CME could not have been forecasted.

Multipoint detections in the inner heliosphere

To understand how this CME evolved through the inner heliosphere, we examine its in situ signatures across the spacecraft located along its path. We performed a coordinated analysis of a 17-spacecraft network in a fortuitous geometric alignment to reconstruct the CME's propagation path and structure within the ecliptic plane.

We focus below on the hidden Earth-directed component that was invisible from Sun-Earth-line remote sensing observations. This component was sampled sequentially by spacecraft near Mercury, Earth, and Mars. We group these observations according to the distinct components of the CME revealed by the multipoint configuration, allowing the geometry of the event to emerge from the combined dataset. Detailed spacecraft-by-spacecraft descriptions and timing information are provided separately (table S2).

BepiColombo (*9*, *10*) first detected the Earth-directed CME component near Mercury (0.35 au) on 16 December 2024 (Fig. 3, BepiColombo). As the structure propagated outward through the Sun-Earth-Mars sector, it affected spacecraft at the first Sun-Earth Lagrange point (L1), within the Earth-Moon system, and later

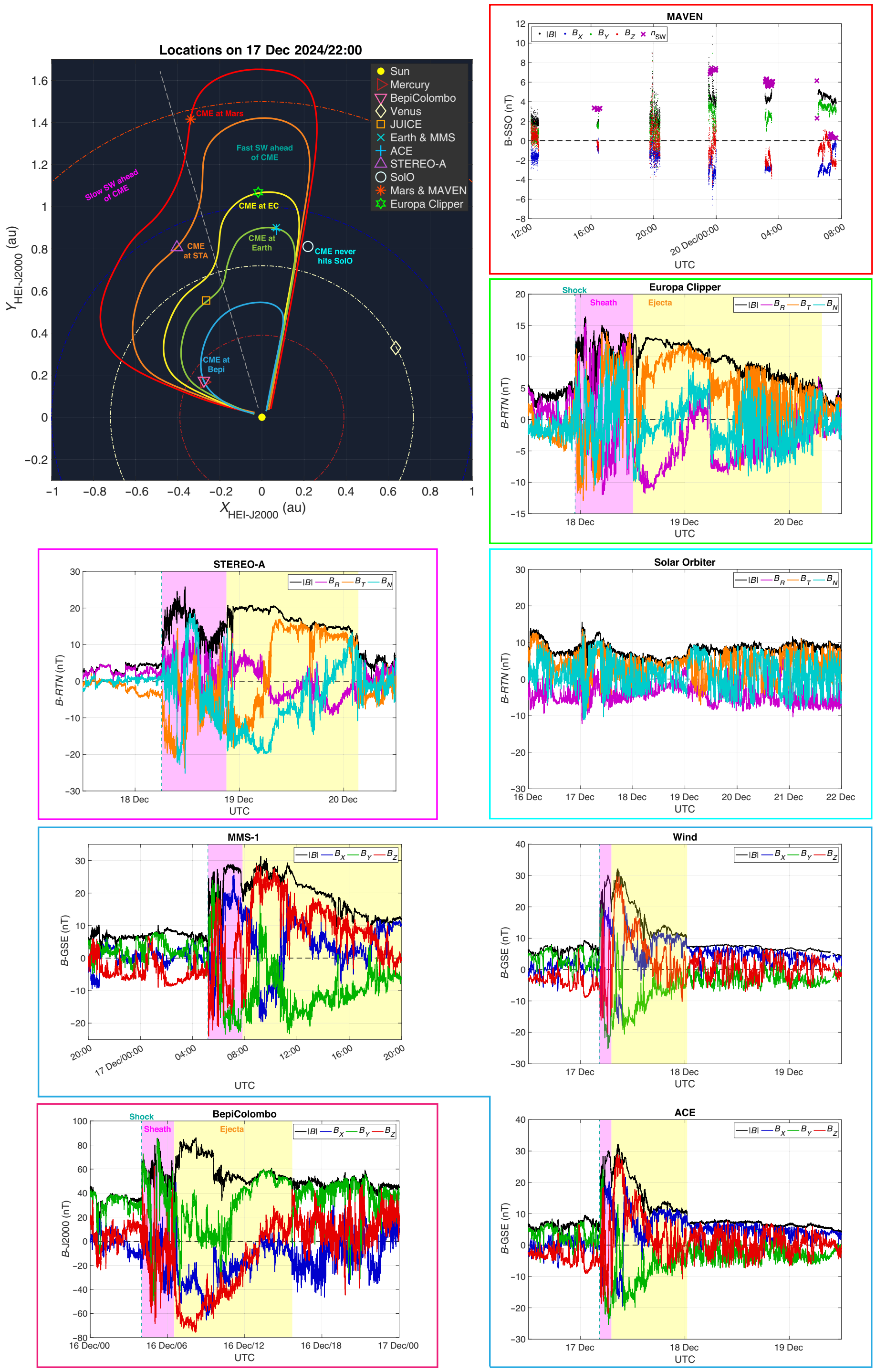

Fig. 3. Multipoint observatory measurements of the CME between 0.35 and 1.6 au. The central panel shows spacecraft locations in the ecliptic plane together with the reconstructed CME structure at five successive times (colored outlines). The shaded regions denote the shock, sheath, and ejecta intervals using the same color scheme as Fig. 1. The reconstruction reveals pronounced longitudinal asymmetry, including a fast Earth-directed lobe and a slower longitudinal flank. Surrounding panels show magnetic field measurements from representative spacecraft across the inner heliosphere, illustrating differences in arrival time, magnetic field strength, and internal structure at each location. Earth-orbiting spacecraft (MMS, Wind, and ACE) are shown in GSE coordinates, whereas deep-space observatories (Europa Clipper, STEREO-A, and Solar Orbiter) are shown in radial-tangential-normal (RTN) coordinates. MAVEN data are presented in Mars-centered coordinates (see Materials and Methods for definitions). Additional magnetic field measurements are provided in the Supplementary Materials. The markedly delayed arrival at STEREO-A, despite its heliocentric distance being comparable to Earth's, together with the absence of a direct encounter at SolO, constrains the longitudinal extent of the Earth-directed component. These multipoint in situ measurements show that the Earth-directed CME component was confined to a limited longitudinal sector and consisted of distinct fast and slow lobes, features that cannot be resolved without off-Sun-Earth-line in situ observations.

between Earth and Mars. Wind, ACE (*11*), and DSCOVR (*12*) at L1 detected the shock on 17 December 2024 (Fig. 3, Wind and ACE; fig. S1), followed by signatures consistent with a turbulent, high-speed sheath, and magnetic cloud.

Within the Earth-Moon system, the four-spacecraft Magnetospheric Multiscale (MMS) Mission (*13*) and the two ARTEMIS (*14*) spacecraft observed a well-defined shock and associated magnetic variability consistent with the same structure. Although MMS and ARTEMIS were located within the same general region of space, observed differences in magnetic configuration reflect local environmental effects rather than separate events (figs. S2 and S3). Europa Clipper subsequently detected the same CME during its cruise phase, sampling the magnetic cloud and its turbulent wake (Fig. 1, A to C).

As the structure continued outward, MAVEN (*15*) recorded a sudden increase in dynamic pressure between 19 December and 20 December, consistent with the passage of the same Earth-directed CME component. Together, these measurements indicate coherent radial propagation of a single CME component through the Sun-Earth-Mars sector over ~2.3 days.

In contrast, STEREO-A, located at nearly the same heliocentric distance as Earth (0.98 au) but displaced in longitude (~29° west of the Sun-Earth line), detected the shock ~25 hours later on 18 December 2024 (Fig. 3, STEREO-A), with a lower solar wind speed sunward of the CME (~400 km s^{-1}). This delayed arrival demonstrates that the Earth-directed CME component did not expand azimuthally as a single, uniform front.

Together, these observations reveal two geometrically distinct aspects of the Earth-directed CME component: a fast lobe passing through the Sun-Earth-Mars sector and a slower longitudinal flank sampled by STEREO-A. These lobes represent different portions of the same asymmetric CME rather than separate events.

A complementary constraint is provided by Solar Orbiter [SolO; (*16*)], positioned ~10° east of the Sun-Earth line at 0.94 au. In contrast to STEREO-A, SolO did not observe a shock or magnetic cloud associated with this event. The absence of a clear CME signature at this longitude limits the eastward extent of the Earth-directed CME.

Together, the delayed arrival at STEREO-A to the west and the nondetection at SolO to the east constrain the longitudinal boundaries of the Earth-directed CME. The observations suggest that the CME was confined to a relatively narrow sector within the ecliptic plane rather than expanding azimuthally as a broad, uniform front. Within this confined CME, the multipoint measurements further reveal asymmetry in the form of fast and slow lobes.

Radial timing and propagation characteristics

Using multipoint in situ observations at various radial distances, we derived the average propagation speed of the Earth-directed CME component (table S3). The results show that the CME's structure was already strongly distorted by the time it reached 1 au. It exhibited a dual-lobe configuration: a fast-propagating lobe that affected Earth, Europa Clipper, and Mars, and a slower lobe that reached STEREO-A roughly a day later (Fig. 3).

The plasma speed between BepiColombo and STEREO-A was significantly lower than between BepiColombo and L1 (table S1), reinforcing the CME's longitudinal asymmetry. The delayed arrival at STEREO-A relative to Earth further supports the presence of a slower lobe in that sector. This pattern is also reflected in the propagation speed derived from STEREO-A to L1 (table S3).

DISCUSSION

Dual-lobe structure and asymmetric propagation

Although BepiColombo and STEREO-A were located within the same longitudinal sector, the CME transit time between them was only slightly longer than that from L1 to Earth. This timing supports the conclusion that the CME comprised two lobes: a faster one propagating along the Sun-Earth-Mars sector and a slower one moving through the longitudinal sector containing Mercury and STEREO-A. Propagation speeds derived from coronagraph observations near the time of the initial shock close to the Sun (Fig. 2D) further reinforce this interpretation. The results also indicate that the CME decelerated as it exchanged momentum with the ambient solar wind while traversing the inner heliosphere (table S3). In the Earth-Mars sector, the CME propagated from the corona to Earth at an average speed of ~840 km s^{-1}, whereas, in the Mercury–STEREO-A sector, its average speed to 1 au was only ~534 km s^{-1}. Between the corona and BepiColombo in that same sector, the CME's average speed was ~566 km s^{-1}, consistent with a dual-lobe, fast-slow configuration. Although the low-level flaring associated with the eruptive filament does not indicate stronger activity on the western side (both exhibited similar C-class flare levels), magnetograms from the days preceding the eruption show that the faster western segment originated in regions of stronger magnetic field, which may explain its higher propagation speed.

The CME did not affect SolO, located only ~10° east of the Sun-Earth line and ~39° east of STEREO-A, providing an additional constraint on the CME's azimuthal extent in the ecliptic plane (Fig. 3). Collectively, these results highlight the strong longitudinal structure of this event. Statistical analyses show that magnetic ejecta near 1 au typically span only ~20° to 30° in longitude, and symmetric signatures across multipoint spacecraft are rare even within this range (*17*). Other multipoint studies report comparable longitudinal variability in magnetic field and energetic particle signatures (*18*), illustrating how rapidly CME properties can vary with heliolongitude. In this context, the present case, where Earth was affected, SolO (10° east) was missed, and STEREO-A (~29° west) encountered a delayed and slower flank, represents longitudinal asymmetry at the extreme end of observed CME variability. The ~25-hour arrival time difference between near-Earth detections and STEREO-A, despite comparable heliocentric distances and in the absence of any additional CME in the ecliptic, cannot be reconciled with a quasi-symmetric expanding front. This pronounced asymmetry reflects distinct fast and slow propagation lobes confined within a narrow, distorted envelope, underscoring the importance of multipoint observations for resolving such geometry.

Forecasting challenges and operational implications

The identification of the hidden CME and its geometry in the ecliptic plane was only possible through coordinated multipoint in situ observations, including vantage points off the Sun-Earth line and spanning a range of heliocentric distances. Because CMEs are among the most significant drivers of space weather, this event highlights a central challenge for space weather forecasting: Without multipoint in situ and remote sensing perspectives, the CME's impact on Earth, Europa Clipper, and Mars would have gone unpredicted. National Oceanic and Atmospheric Administration's Daily Solar Geophysical Activity Report and Forecast did not mention this CME or its associated filament eruption. A contemporaneous SWPC forecast discussion issued on 15 December 2024 briefly referenced the eruption, describing a large, southward-directed CME expected to miss Earth and propagate upstream. The Earth-directed hidden component identified in this study was neither forecasted nor recognized in operational analyses, demonstrating how such components can escape detection when viewed solely from the Sun-Earth line. Similar events have shown that even well-observed eruptions can appear undetectable or mischaracterized from that perspective (*18*). This limitation is particularly consequential in the region between Earth and Mars, where Europa Clipper effectively served as a proxy for future crewed missions.

The pronounced longitudinal asymmetry revealed by this event provides a stringent case for ensemble magnetohydrodynamics propagation models (*19*–*22*). Evaluating whether ensemble members reproduce the observed narrow, fast-lobe structure would directly assess the capability of current forecasting frameworks to capture such asymmetric evolution.

Future directions
Previous large-scale CME studies have tracked CME propagation from 1 au to beyond 30 au using up to 10 spacecraft, of which six were located in the inner heliosphere (*23*, *24*). In comparison, the present analysis uses data from 17 in situ and remote sensing observatories distributed between 0.35 and 1.5 au, providing the most detailed coverage to date of a CME's radial and longitudinal evolution within the inner heliosphere. The 1- to 1.5-au region remains little explored and represents a critical knowledge gap for heliophysics and space weather research (*25*). Nonetheless, a few recent studies have examined CME evolution between Earth and Mars (*26*, *27*), reinforcing the importance of multipoint observations in this part of the heliosphere.

Fast CMEs often drive interplanetary shocks capable of accelerating solar energetic particles to high energies. These particles can penetrate spacecraft shielding and pose acute radiation risks to astronauts during interplanetary transit or lunar surface operations. In addition, enhanced dynamic pressure and magnetic disturbances can disrupt spacecraft systems and communication. Forecasts missing Earth- or Mars-directed CMEs, therefore, have direct implications for crew safety and operational planning.

Our results further demonstrate the value of maintaining magnetometer, plasma, and particle instruments operational on planetary missions such as Europa Clipper, BepiColombo, and JUICE during their interplanetary cruise phases (*26*, *27*). At the time of this event, JUICE (*28*) was not collecting solar wind data. Contemporaneous cruise-phase measurements would have provided an additional longitudinal constraint on the slow lobe of the Earth-directed component (Fig. 3).

While this extensive dataset offers a uniquely detailed view of this CME's evolution, some limitations remain. The spatial distribution of observatories, although dense within the inner heliosphere, was uneven, leaving gaps in latitudinal coverage and limited sampling of magnetic field orientations. Because all measurements were obtained within or near the ecliptic plane, this analysis cannot fully resolve the CME's three-dimensional structure or vertical extent. Expanding this approach to additional CMEs with varying morphologies and source regions will help determine how common dual-lobed or similarly complex structures are.

Future missions positioned off the Sun-Earth line, such as the European Space Agency's upcoming Vigil mission at the Sun-Earth L5 point (located ~60° behind Earth in its orbit), together with continued operation of planetary cruise-phase instruments, will be key to filling spatial gaps and testing the generality of these results. Such capabilities will also strengthen space-weather forecasting and enhance astronaut safety. Leveraging planetary missions for heliophysics objectives aligns with the integrated science vision outlined in the Solar and Space Physics Decadal Survey (*29*).

This study demonstrates the power of coordinated multipoint observations to uncover the true complexity of CME evolution in the inner heliosphere. Capturing a single event with 17 observatories spanning 0.35 to 1.5 au revealed that one CME in the ecliptic evolved as a longitudinally structured, dual-lobe system rather than as a uniformly expanding "bubble." Such structure would not have been resolvable from Sun-Earth line observations alone. As human exploration extends toward Mars, such comprehensive heliospheric coverage will be critical for protecting spacecraft and crew. Continued multipoint monitoring will be vital to predicting the Sun's dynamic behavior and its effects on our human systems.

MATERIALS AND METHODS
Experimental design
The objective of this study was to characterize a CME observed across the inner heliosphere and to interpret the plasma and magnetic field measurements obtained by the PIMS and the ECM on NASA's Europa Clipper spacecraft during its interplanetary cruise. Multipoint observations from 17 spacecraft were used to analyze CME propagation, timing, and structure between 0.35 and 1.6 au. Imaging data from SOHO, STEREO-A, and Solar Dynamics Observatory (SDO) were combined with in situ measurements to reconstruct the CME in three dimensions using the Graduated Cylindrical Shell (GCS) model.

Coordinate systems and reference frames
Magnetic field measurements from the 17 spacecraft are presented in the coordinate systems customarily used for each mission. For Earth-orbiting observatories (MMS, Wind, and ACE), data are shown in geocentric solar ecliptic (GSE) coordinates. For deep-space observatories (Europa Clipper, STEREO-A, and SolO), measurements are displayed in radial-tangential-normal (RTN) coordinates. MAVEN data near Mars are presented in Mars-centered solar orbital (MSO/SSO) coordinates, while BepiColombo data near Mercury are show in ecliptic J2000 coordinates.

For earth-based observatories, GSE coordinates are directly comparable to RTN coordinates, with the X_{GSE} axis approximately antiparallel to the radial ($-R$) direction, Y_{GSE} corresponding to $-T$, and Z_{GSE} corresponding to N. Because each spacecraft operates in a distinct heliocentric and planetary reference frame, data are presented in mission-standard coordinates for clarity and consistency with published instrument calibrations.

For direct comparisons between spacecraft, differences in coordinate systems are accounted for in the interpretation rather than through global coordinate transformation.

Three-dimensional reconstruction of the CME
To explain the significant differences in in situ arrival times, we reconstructed the CME in three dimensions using the GCS model (*30*). The GCS model represents a geometric depiction of a magnetic flux rope, the fundamental magnetic structure of a CME (*31*). The model comprises a cylindrical shell representing the CME body

attached to two cones representing its "legs." It includes six free parameters: three describing position (Carrington longitude, latitude, and tilt angle) and three describing shape (angular width, aspect ratio, and heliocentric height of the front).

Parameters were iteratively adjusted to achieve visual agreement between the model and coronagraphic observations from SOHO/LASCO C3 and STEREO-A/SECCHI (COR2A, HI1, and HI2), using data collected between 15 December 05:00 UT and 18 December 06:00 UT. Because of the CME's highly asymmetric nature, two GCS components were required to reproduce its geometry (cyan and green wireframes in Fig. 2). This approach enabled characterization of both the southward-directed and Earth-directed lobes and provided insight into their physical interactions.

The GCS model has been extensively validated (*32–34*) and applied in over 400 studies since 2009. Here, it provided a framework for quantifying deviations from an idealized flux rope, offering context for the observed timing discrepancies across the heliosphere.

Propagation speed calculation

We calculated the average CME propagation speeds between pairs of spacecraft using a timing analysis based on the observed shock or magnetic cloud arrival times. For each spacecraft pair, we determined the time difference (Δt) between the leading edge or shock detections and divided it by the difference in heliocentric distance assuming a radially outbound CME propagation path (ΔR)

$$v_{\text{avg}} = \frac{\Delta R}{\Delta t}$$

We identified the arrival times from in situ plasma and magnetic field signatures, including abrupt increases in density, dynamic pressure, and magnetic field strength. We retrieved heliocentric distances from spacecraft ephemerides.

We estimated uncertainties in the calculated speeds from two primary sources: (i) the precision of the recorded arrival times, which typically ranges from <1 s to hours (only in the case of MAVEN at Mars), and (ii) the spacecraft positions relative to the CME front. We also used the coronagraph data to generate a time estimate for the shock in the corona at 10 solar radii and a hemispherical shock geometry. We propagated these uncertainties throughout the calculation to obtain an average error of ±32 km s^{-1} for all derived speeds (table S3). The derived speeds are consistent with in situ observations of the bulk plasma flows.

Supplementary Materials

The PDF file includes:
Supplementary Text
Figs. S1 to S6
Tables S1 to S3
Legend for data file S1

Other Supplementary Material for this manuscript includes the following:
Data file S1

REFERENCES

1. R. T. Pappalardo, B. J. Buratti, H. Korth, D. A. Senske, D. L. Blaney, D. D. Blankenship, J. L. Burch, P. R. Christensen, S. Kempf, M. G. Kivelson, E. Mazarico, K. D. Retherford, E. P. Turtle, J. H. Westlake, B. G. Paczkowski, T. L. Ray, J. Kampmeier, K. L. Craft, S. M. Howell, R. L. Klima, E. J. Leonard, A. Matiella Novak, C. B. Phillips, I. J. Daubar, J. Blacksberg, S. M. Brooks, M. N. Choukroun, C. J. Cochrane, S. Diniega, C. M. Elder, C. M. Ernst, M. S. Gudipati, A. Luspay-Kuti, S. Piqueux, A. M. Rymer, J. H. Roberts, G. Steinbrügge, M. L. Cable, J. E. C. Scully, J. C. Castillo-Rogez, H. C. F. C. Hay, D. M. Persaud, C. R. Glein, W. B. McKinnon, J. M. Moore, C. A. Raymond, D. M. Schroeder, S. D. Vance, D. Y. Wyrick, M. Y. Zolotov, K. P. Hand, F. Nimmo, M. A. McGrath, J. R. Spencer, J. I. Lunine, C. S. Paty, J. M. Soderblom, G. C. Collins, B. E. Schmidt, J. A. Rathbun, E. L. Shock, T. C. Becker, A. G. Hayes, L. M. Prockter, B. P. Weiss, C. A. Hibbitts, A. Moussessian, T. G. Brockwell, H.-W. Hsu, X. Jia, G. R. Gladstone, A. S. McEwen, G. W. Patterson, R. L. McNutt Jr., J. P. Evans, T. W. Larson, L. A. Cangahuala, G. G. Havens, B. B. Buffington, B. Bradley, S. Campagnola, S. H. Hardman, J. M. Srinivasan, K. L. Short, T. C. Jedrey, J. A. St. Vaughn, K. P. Clark, J. Vertesi, C. Niebur, Science overview of the Europa Clipper mission. *Space Sci. Rev.* **220**, 40 (2024).
2. J. H. Westlake, R. L. McNutt Jr., M. Grey, D. Coren, A. M. Rymer, C. J. Cochrane, A. Luspay-Kuti, E. Hohlfeld, N. Seese, A. Crew, S. Liang, T. Diaz, H. T. Smith, C. Shearer, K. E. Mandt, K. Asmar, K. Cooper, C. Battista, C. Kim, S. Katz, M. Kusterer, L. Brown, D. Linko, C. Schlemm, S. Jaskulek, J. Dalton, R. Caranza, E. Reynolds, M. Richardson, J. Saur, N. Krupp, E. Roussos, The Plasma Instrument for Magnetic Sounding (PIMS) on the Europa Clipper mission. *Space Sci. Rev.* **219**, 62 (2023).
3. M. G. Kivelson, X. Jia, K. A. Lee, C. A. Raymond, K. K. Khurana, M. O. Perley, J. B. Biersteker, J. Blacksberg, R. Caron, C. J. Cochrane, O. R. Dawson, C. D. K. Harris, J. E. Jones, S. Joy, H. Korth, J. Liu, E. Maghsoudi, N. Murphy, D. Parsley, D. R. Pierce, C. Racho, I. Richter, C. T. Russell, S. Sherman, R. J. Strangeway, M. Villarreal, B. P. Weiss, L. Wigglesworth, The Europa Clipper Magnetometer. *Space Sci. Rev.* **219**, 48 (2023).
4. C. J. Cochrane, S. P. Joy, H. Korth, J. B. Biersteker, J. Blacksberg, M. Bouchard, J. Contreras, O. R. Dawson, K. K. Khurana, N. Murphy, D. Palm, M. O. Perley, D. R. Pierce, I. Richter, C. T. Russell, S. Sherman, R. J. Strangeway, B. P. Weiss, L. Wigglesworth, M. G. Kivelson, X. Jia, C. A. Raymond, Europa Clipper Magnetometer boom deployment: A first look at the magnetometer observations of the spacecraft and the interplanetary magnetic field. *Space Sci. Rev.* **221**, 115 (2025).
5. C. Larrodera, C. Cid, Bimodal distribution of the solar wind at 1 AU. *Astron. Astrophys.* **635**, A44 (2020).
6. L. B. Wilson III, A. L. Brosius, J. C. Kasper, M. L. Stevens, P. S. Miralles, L. K. Jian, J. L. Steinberg, J. T. Steinberg, The statistical properties of solar wind temperature parameters near 1 au. *Astrophys. J. Suppl. Ser.* **236**, 41 (2018).
7. V. Domingo, B. Fleck, A. I. Poland, The SOHO mission: An overview. *Sol. Phys.* **162**, 1–37 (1995).
8. M. L. Kaiser, T. A. Kucera, J. M. Davila, O. C. St. Cyr, M. Guhathakurta, E. Christian, The STEREO mission: An Introduction. *Space Sci.* **136**, 5–16 (2008).
9. J. Benkhoff, G. Murakami, W. Baumjohann, S. Besse, E. Bunce, M. Casale, G. Cremosese, K.-H. Glassmeier, H. Hayakawa, D. Heyner, H. Hiesinger, J. Huovelin, H. Hussmann, V. Iafolla, L. Iess, Y. Kasaba, M. Kobayashi, A. Milillo, I. G. Mitrofanov, E. Montagnon, M. Novara, S. Orsini, E. Quemerais, U. Reininghaus, Y. Saito, F. Santoli, D. Stramaccioni, O. Sutherland, N. Thomas, I. Yoshikawa, J. Zender, BepiColombo - Mission overview and science goals. *Space Sci. Rev.* **217**, 90 (2021).
10. D. Heyner, H.-U. Auster, K.-H. Fornaçon, C. Carr, I. Richter, J. Z. D. Mieth, P. Kolhey, W. Exner, U. Motschmann, W. Baumjohann, A. Matsuoka, W. Magnes, G. Berghofer, D. Fischer, F. Plaschke, R. Nakamura, Y. Narita, M. Delva, M. Volwerk, A. Balogh, M. Dougherty, T. Horbury, B. Langlais, M. Mandea, A. Masters, J. S. Oliveira, B. Sánchez-Cano, J. A. Slavin, S. Vennerstrøm, J. Vogt, J. Wicht, K.-H. Glassmeier, The BepiColombo planetary magnetometer MPO-MAG: What can we learn from the Hermean magnetic field? *Space Sci. Rev.* **217**, 52 (2021).
11. E. C. Stone, A. M. Frandsen, R. A. Mewaldt, E. R. Christian, D. Margolies, J. F. Ormes, F. Snow, The advanced composition explorer. *Space Sci. Rev.* **86**, 1–22 (1998).
12. J. Burt, B. Smith, "Deep space climate observatory: The DSCOVR mission," in *2012 IEEE Aerospace Conference* (IEEE, 2012), pp. 1–13.
13. J. L. Burch, T. E. Moore, R. B. Torbert, B. L. Giles, Magnetospheric multiscale overview and science objectives. *Space Sci. Rev.* **199**, 5–21 (2016).
14. V. Angelopoulos, The ARTEMIS mission. *Space Sci. Rev.* **165**, 3–25 (2011).
15. B. M. Jakosky, R. P. Lin, J. M. Grebowsky, J. G. Luhmann, D. F. Mitchell, G. Beutelschies, T. Priser, M. Acuña, L. Andersson, D. Baird, D. Baker, R. Bartlett, M. Benna, S. Bougher, D. Brain, D. Carson, S. Cauffman, P. Chamberlin, J.-Y. Chaufray, O. Cheatom, J. Clarke, J. Connerney, T. Cravens, D. Curtis, G. Delory, S. Demcak, A. DeWolfe, F. Eparvier, R. Ergun, A. Eriksson, J. Espley, X. Fang, D. Folta, J. Fox, C. Gomez-Rosa, S. Habenicht, J. Halekas, G. Holsclaw, M. Houghton, R. Howard, M. Jarosz, N. Jedrich, M. Johnson, W. Kasprzak, M. Kelley, T. King, M. Lankton, D. Larson, F. Leblanc, F. Lefevre, R. Lillis, P. Mahaffy, C. Mazelle, W. McClintock, J. McFadden, D. L. Mitchell, F. Montmessin, J. Morrissey, W. Peterson, W. Possel, J.-A. Sauvaud, N. Schneider, W. Sidney, S. Sparacino, A. I. F. Stewart, R. Tolson, D. Toublanc, C. Waters, T. Woods, R. Yelle, R. Zurek, The Mars Atmosphere and Volatile Evolution (MAVEN) mission. *Space Sci. Rev.* **195**, 3–48 (2015).
16. D. Müller, O. C. St. Cyr, I. Zouganelis, H. R. Gilbert, R. Marsden, T. Nieves-Chinchilla, E. Antonucci, F. Auchère, D. Berghmans, T. S. Horbury, R. A. Howard, S. Krucker, M. Maksimovic, C. J. Owen, P. Rochus, J. Rodriguez-Pacheco, M. Romoli, S. K. Solanki, R. Bruno, M. Carlsson, A. Fludra, L. Harra, D. M. Hassler, S. Livi, P. Louarn, H. Peter, U. Schühle, L. Teriaca, J. C. del Toro Iniesta, R. F. Wimmer-Schweingruber, E. Marsch, M. Velli, A. De Groof, A. Walsh, D. Williams, The Solar Orbiter mission: Science overview. *Astron. Astrophys.* **642**, A1 (2020).

17. N. Lugaz, B. Zhuang, C. Scolini, N. Al-Haddad, C. J. Farrugia, R. M. Winslow, F. Regnault, C. Möstl, E. E. Davies, A. B. Galvin, The width of magnetic ejecta measured near 1 au: Lessons from STEREO-A measurements in 2021–2022. *Astrophys. J.* **962**, 193 (2024).
18. J. L. F. von Forstner, M. Dumbović, C. Möstl, J. Guo, A. Papaioannou, R. Elftmann, Z. Xu, J. C. Terasa, A. Kollhoff, R. F. Wimmer-Schweingruber, J. Rodríguez-Pacheco, A. J. Weiss, J. Hinterreiter, T. Amerstorfer, M. Bauer, A. V. Belov, Radial evolution of the April 2020 stealth coronal mass ejection between 0.8 and 1 AU: Comparison of Forbush decreases at Solar Orbiter and near the Earth. *Astron. Astrophys.* **656**, A1 (2021).
19. E. Palmerio, C. Kay, N. Al-Haddad, B. J. Lynch, D. Trotta, W. Yu, V. E. Ledvina, B. Sánchez-Cano, P. Riley, D. Heyner, D. Schmid, D. Fischer, I. Richter, H.-U. Auster, A coronal mass ejection encountered by four spacecraft within 1 AU from the Sun: Ensemble modelling of propagation and magnetic structure. *Mon. Not. R. Astron. Soc.* **536**, 203–222 (2025).
20. D. Odstrčil, P. Riley, J. A. Linker, R. Lionello, Z. Mikić, V. J. Pizzo, "3-D simulations of ICMEs by coupled coronal and heliospheric models," in *Solar Variability as an Input to the Earth's Environment, ESA SP-535* (European Space Agency, 2003), pp. 541–546.
21. J. Pomoell, S. Poedts, EUHFORIA: European heliospheric forecasting information asset. *J. Space Weather Space Clim.* **8**, A35 (2018).
22. M. L. Mays, A. Taktakishvili, A. Pulkkinen, P. J. MacNeice, L. Rastätter, D. Odstrcil, L. K. Jian, I. G. Richardson, J. A. LaSota, Y. Zheng, M. M. Kuznetsova, Ensemble modeling of CMEs using the WSA–ENLIL+Cone model. *Sol. Phys.* **290**, 1775–1814 (2015).
23. O. Witasse, B. Sánchez-Cano, M. L. Mays, P. Kajdič, H. Opgenoorth, H. A. Elliott, I. G. Richardson, I. Zouganelis, J. Zender, R. F. Wimmer-Schweingruber, L. Turc, M. G. G. T. Taylor, E. Roussos, A. Rouillard, I. Richter, J. D. Richardson, R. Ramstad, G. Provan, A. Posner, J. J. Plaut, D. Odstrcil, H. Nilsson, P. Niemenen, S. E. Milan, K. Mandt, H. Lohf, M. Lester, J.-P. Lebreton, E. Kuulkers, N. Krupp, C. Koenders, M. K. James, D. Intzekara, M. Holmstrom, D. M. Hassler, B. E. S. Hall, J. Guo, R. Goldstein, C. Goetz, K. H. Glassmeier, V. Génot, H. Evans, J. Espley, N. J. T. Edberg, M. Dougherty, S. W. H. Cowley, J. Burch, E. Behar, S. Barabash, D. J. Andrews, N. Altobelli, Interplanetary coronal mass ejection observed at STEREO-A, Mars, comet 67P/Churyumov-Gerasimenko, Saturn, and New Horizons en route to Pluto: Comparison of its Forbush decreases at 1.4, 3.1, and 9.9 AU. *J. Geophys. Res. Space Phys.* **122**, 7865–7890 (2017).
24. C. Larrodera, M. Temmer, Evolution of coronal mass ejections with and without sheaths from the inner to the outer heliosphere: Statistical investigation for 1975 to 2022. *Astron. Astrophys.* **685**, A89 (2024).
25. C. O. Lee, B. Sánchez-Cano, G. A. DiBraccio, M. Mayyasi, S. Xu, P. Chamberlin, E. Davies, C. Scolini, R. J. Filwett, R. Ramstad, E. Palmerio, B. J. Lynch, J. G. Luhmann, B. Ehresmann, J. Guo, R. C. Allen, S. Vines, R. Winslow, H. Elliott, Heliophysics and space weather science at ∼1.5 AU: Knowledge gaps and need for space weather monitors at Mars. *Front. Astron. Space Sci.* **10**, 1064208 (2023).
26. C. Möstl, A. J. Weiss, M. A. Reiss, T. Amerstorfer, R. L. Bailey, J. Hinterreiter, M. Bauer, D. Barnes, J. A. Davies, R. A. Harrison, J. L. Freiherr von Forstner, E. E. Davies, D. Heyner, T. Horbury, S. D. Bale, Multipoint interplanetary coronal mass ejections observed with Solar Orbiter, BepiColombo, Parker Solar Probe, Wind, and STEREO-A. *Astrophys. J. Lett.* **924**, L6 (2022).
27. B. Sánchez-Cano, L. Z. Hadid, S. Aizawa, G. Murakami, Y. Bamba, S. Chiba, T. Hara, D. Heyner, G. Ho, K. Iwai, E. Kilpua, G. Kinoshita, B. Lavraud, Y. Miyoshi, M. Pinto, D. Schmid, D. Shiota, R. Vainio, N. Andre, A. Aronica, S. Asmar, H.-U. Auster, S. Barabash, A. Barthe, W. Baumjohann, J. Benkhoff, M. Bentley, E. Bunce, P. Cappuccio, D. Delcourt, I. di Stefano, I. Doria, N. Dresing, A. Fedorov, D. Fischer, B. Fiethe, M. Fränz, J. Gieseler, F. Giner, G. Giono, Y. Harada, H. Hussmann, L. Iess, T. Imamura, H. Jeszenszky, G. Jones, B. Katra, A. Kazakov, A. Kozyrev, G. Laky, C. Lefevre, H. Lichtenegger, S. Lindsay, M. Lucente, C. Magnafico, W. Magnes, A. Martindale, A. Matsuoka, A. Milillo, I. Mitrofanov, G. Nishiyama, P. Oleynik, S. Orsini, M. Paik, C. Palmroos, C. Plainaki, E. Penou, M. Persson, F. Quarati, E. Quémerais, I. Richter, R. Robidel, M. Rojo, Y. Saito, F. Santoli, A. Stark, M. Stumpo, R. Tian, A. Varsani, C. Verdeil, H. Williamson, O. Witasse, S. Yokota, BepiColombo cruise science: Overview of the mission contribution to heliophysics. *Earth Planets Space* **77**, 114 (2025).
28. O. Grasset, M. K. Dougherty, A. Coustenis, E. J. Bunce, C. Erd, D. Titov, M. Blanc, A. Coates, P. Drossart, L. N. Fletcher, H. Hussmann, R. Jaumann, N. Krupp, J.-P. Lebreton, O. Prieto-Ballesteros, P. Tortora, F. Tosi, T. Van Hoolst, JUpiter ICy moons Explorer (JUICE): An ESA mission to orbit Ganymede and to characterise the Jupiter system. *Planet. Space Sci.* **78**, 1–21 (2013).
29. National Academies of Sciences, Engineering, and Medicine, *Solar and Space Physics: A Decadal Strategy for Solar and Space Physics (Heliophysics) 2024–2033* (National Academies Press, 2024).
30. A. F. R. Thernisien, R. A. Howard, A. Vourlidas, Modeling of flux rope coronal mass ejections. *Astrophys. J.* **652**, 763–773 (2006).
31. J. Chen, Theory of prominence eruption and propagation: Interplanetary consequences. *J. Geophys. Res.* **101**, 27499–27520 (1996).
32. A. Vourlidas, P. Subramanian, K. P. Dere, R. A. Howard, Large-angle spectrometric coronagraph measurements of the energetics of coronal mass ejections. *Astrophys. J.* **534**, 456–467 (2000).
33. A. Thernisien, A. Vourlidas, R. A. Howard, CME reconstruction: Pre-STEREO and STEREO era. *J. Atmos. Sol.-Terr. Phys.* **73**, 1156–1165 (2011).
34. K. Martinić, B. Vršnak, M. Dumbović, J. Čalogović, M. Temmer, A. Veronig, Determination of coronal mass ejection orientation and consequences for their propagation. *Astro. Astrophys.* **661**, A155 (2022).

Acknowledgments: We thank T. Horbury for providing the Solar Orbiter magnetometer data, S. Joy for contributions to the ECM data production, and J. Epsley and D. Mitchell for work on the MAVEN data used in this study. **Funding:** This work was supported by the National Aeronautics and Space Administration (NASA) and other sources as follows: NASA subcontract 1715071 from the Jet Propulsion Laboratory, California Institute of Technology (A.L.-K., A.B.C., R.L.M., H.T.S., D.W., T.A.N., and A.M.R.); NASA subcontract 1711220 from the Jet Propulsion Laboratory, California Institute of Technology (D.L.T. and H.K.); NASA contract 80NM0018D0004 at the Jet Propulsion Laboratory, California Institute of Technology (C.J.C., C.A.R., J.S., M.G.K., and K.K.K.); NASA grant 80NSSC22K0970 (E.P. and A.V.); Johns Hopkins University Applied Physics Laboratory Independent Research and Development funding (S.R.); NASA subcontract 193072 from the Johns Hopkins University Applied Physics Laboratory (X.Z. and J.A.S.); NASA subcontract 193078 from the Johns Hopkins University Applied Physics Laboratory (M.L.S.); NASA contract 80NSSC22K0225 supporting consultation related to the Wind SWE Faraday Cup experiment (M.L.S.); NASA subcontract 195680 from the Johns Hopkins University Applied Physics Laboratory (M.H.K. and K.K.K.); NASA subcontract 193016 from the Johns Hopkins University Applied Physics Laboratory (C.S.P.); NASA contract NNH10CC04C (K.H., A.M.R., J.R.G., J.S.H., and S.M.C.); and German Ministerium für Wirtschaft und Klimaschutz and the German Zentrum für Luft- und Raumfahrt under contract 50QW2202 (D.H.). **Author contributions:** Conceptualization: A.L.-K., D.L.T., A.V., R.L.M., J.H.W., H.K., H.T.S., J.A.S., T.A.N., and K.K.K. Methodology: A.L.-K., D.L.T., A.V., A.B.C., R.L.M., J.H.W., H.K., H.T.S., J.A.S., and T.A.N. Software: A.L.-K., D.L.T., C.J.C., A.R., and K.H. Validation: A.L.-K., E.P., A.B.C., D.L.T., A.V., J.S.H., C.J.C., C.A.R., A.R., E.R., and M.L.S. Formal analysis: A.L.-K., D.L.T., E.P., A.V., A.B.C., R.L.M., C.J.C., X.J., D.W., M.L.S., H.T.S., K.E.M., and T.A.N. Investigation: A.L.-K., D.L.T., E.P., A.V., A.B.C., R.L.M., J.H.W., C.J.C., X.J., C.A.R., J.R.G., S.M.C., H.T.S., M.L.S., J.A.S., D.H., K.E.M., D.W., C.S.P., A.M.R., and E.R. Resources: A.L.-K., D.L.T., A.V., S.R., J.H.W., C.J.C., X.J., C.A.R., D.H., A.R., J.R.G., J.S.H., S.M.C., M.G.K., and M.L.S. Data curation: A.L.-K., D.L.T., E.P., C.J.C., K.H., D.W., X.J., D.H., J.S.H., A.R., and M.L.S. Writing—original draft: A.L.-K., D.L.T., E.P., A.V., A.B.C., S.R., C.J.C., X.J., H.K., E.R., K.E.M., and T.A.N. Writing—review and editing: A.L.-K., D.L.T., E.P., A.V., A.B.C., S.R., C.J.C., X.J., C.A.R., J.H.W., H.K., J.A.S., M.G.K., K.K.K., H.T.S., D.H., E.R., K.E.M., N.K., D.W., J.S., T.A.N., and K.H. Visualization: D.L.T., E.P., and A.L.-K. Supervision: A.L.-K. and A.V. Project administration: A.L.-K. and J.H.W. Funding acquisition: A.L.-K., M.G.K., C.S.P., J.A.S., C.A.R., and D.H. **Competing interests:** The authors declare that they have no competing interests. **Data, code, and materials availability:** All data and code needed to evaluate and reproduce the results in the paper are present in the paper and/or the Supplementary Materials. This study did not generate new materials. Publicly available datasets used in this study can be accessed through mission archives, including NASA's Coordinated Data Analysis Web (CDAWeb; https://cdaweb.gsfc.nasa.gov/), the NASA Planetary Data System (PDS; https://pds.nasa.gov/), and the European Space Agency's Planetary Science Archive (PSA; https://psa.esa.int/), as applicable to each mission. Supplementary Data File S1 is a ZIP archives containing all magnetic field time series used in this analysis. Each CSV file includes UTC timestamps, magnetic field magnitude, and vector magnetic field components in the coordinate system specified in the file name and column headers. The archive also includes a README.txt file describing the data columns and a MANIFEST.csv file listing the spacecraft, coordinate system, time interval, contents, and units for each file. Spacecraft positions, shock arrival times, and derived propagation speeds used in the reconstruction are provided in the Supplementary Materials.

Submitted 24 November 2025
Accepted 29 June 2026
Published 19 August 2026
10.1126/sciadv.aed9960

Science Advances

The structure of a complex, asymmetric coronal mass ejection revealed by 17 spacecraft across the inner heliosphere

Adrienn Luspay-Kuti, Drew L. Turner, Evangelos Paouris, Angelos Vourlidas, Alexander B. Crew, Ralph L. McNutt, Joseph H. Westlake, Savvas Raptis, Corey J. Cochrane, Xianzhe Jia, Carol A. Raymond, Haje Korth, Daniel Heyner, Kathleen Hanley, Ali Rahmati, Jacob R. Gruesbeck, Jasper S. Halekas, Shannon M. Curry, Howard Todd Smith, Michael L. Stevens, Elias Roussos, Kathleen E. Mandt, Margaret G. Kivelson, James A. Slavin, Dany Waller, Krishan K. Khurana, Tom Andre Nordheim, Carol S. Paty, Abigail M. Rymer, Joachim Saur, and Norbert Krupp

Sci. Adv. **12** (34), eaed9960. DOI: 10.1126/sciadv.aed9960

Science Advances (ISSN 2375-2548) is published by the American Association for the Advancement of Science. 1200 New York Avenue NW, Washington, DC 20005. The title *Science Advances* is a registered trademark of AAAS.